

# Induced radioactivity in CMS

**Mika Huhtinen**

CERN, CH-1211 Geneva, Switzerland

## ABSTRACT

This document summarises the induced activity dose rates predicted for the CMS experiment at the CERN LHC collider. The computational methods are shortly described and some comparisons to experimental data are given. The shielding optimisation of the most activated object – the CMS forward calorimeter – is described in great detail in order to illustrate the methods. The dose rates around other components of CMS are presented, followed by some discussion about need and possible implementation of shielding measures.

# 1 Introduction

In the design of the CMS experiment an effort has been made to take into account radiological safety aspects from the very beginning. When CMS is closed the detector itself and the forward shielding provide a hermetic enclosure around all activated elements and – as will be shown – the dose rates in the UXC cavern due to induced radioactivity are close to normal natural levels. When CMS or the forward shielding are opened, parts of the beam-line, shielding elements or calorimeters get freely exposed. These can have induced activity levels, which lead to contact dose rates in the mSv/h range. Regions of such high activity are always very localized. The most active elements will be the TAS absorbers at each end of the experimental cavern. In CMS these are embedded in shielding and normally not accessible. Other highly activated elements are the high- $\eta$  edges of the end-cap calorimeters (EE and HE) and, especially, the forward calorimeter (HF). For the latter a special storage and maintenance garage is foreseen and the optimisation of a dedicated shielding is described in this note. Also the beam-pipe, even though it is a thin object, can locally reach contact dose rates in the mSv/h regime and will require special attention with respect to personnel protection.

Since the most radioactive regions in CMS are fairly well localized, efficient protection can be provided by either some dedicated local shielding or by imposing a sufficient safety distance. For instance, if the activated region of a calorimeter surface would have an area of  $1 \text{ m}^2$  with a contact dose rate of  $1 \text{ mSv/h}$ , then the dose rate at  $3 \text{ m}$  distance would be about  $20 \text{ } \mu\text{Sv/h}$ , only.

In practice the contact doses of calorimeters and shielding elements change gradually because the hadron flux emerging from the interaction point – and representing the primary source of activation – follows roughly a  $1/r^2$  dependence, where  $r$  is the distance to the beam-line<sup>1</sup>. Thus protection will be a tradeoff of dedicated shielding in the regions of highest activity and weight of the shielding. The latter can impose significant complications in the installation and thus might even increase the exposure of personnel.

In addition to distance and dedicated shielding a third method of protection is to minimise the time spent in areas with high dose rate. Provided that maintenance operations are designed to be fast, they can be performed even in regions with several mSv/h dose rate. In some cases a design for a fast intervention can be preferable to a lengthy operation of installing temporary shielding.

In order to guide the design of shielding and maintenance operations, it has been agreed to set a *design limit* of  $5 \text{ mSv}$  for the annual whole body exposure of an individual person<sup>2</sup>. This limit is by a factor of 3 lower than the present official annual limit of CERN [1]. This  $5 \text{ mSv}$  limit only serves as a simple guideline to design operations and temporary shielding. It will allow to identify cases where, e.g., maintenance of detectors might become critical due to a need to spend long times in high or moderate dose rate environments. For instance, this  $5 \text{ mSv}$  implies that one person can work a maximum of 100 hours a year in a region with  $50 \text{ } \mu\text{Sv/h}$  dose rate. Of course, irrespective of any limits, the ALARA (As Low As Reasonably Achievable) principle must be followed in all of the design.

---

<sup>1</sup>Indeed, the fluxes depend on the distance to the beam-line and not to the interaction point. In the absence of magnetic fields this follows analytically from the fact that the particle density is uniform in pseudorapidity  $\eta = -\ln \tan(\theta/2)$  and *not* in polar angle  $\theta$ .

<sup>2</sup>The dose allowance for hands and feet is much higher, therefore this  $5 \text{ mSv}$  limit should normally not be applied to contact dose rates.

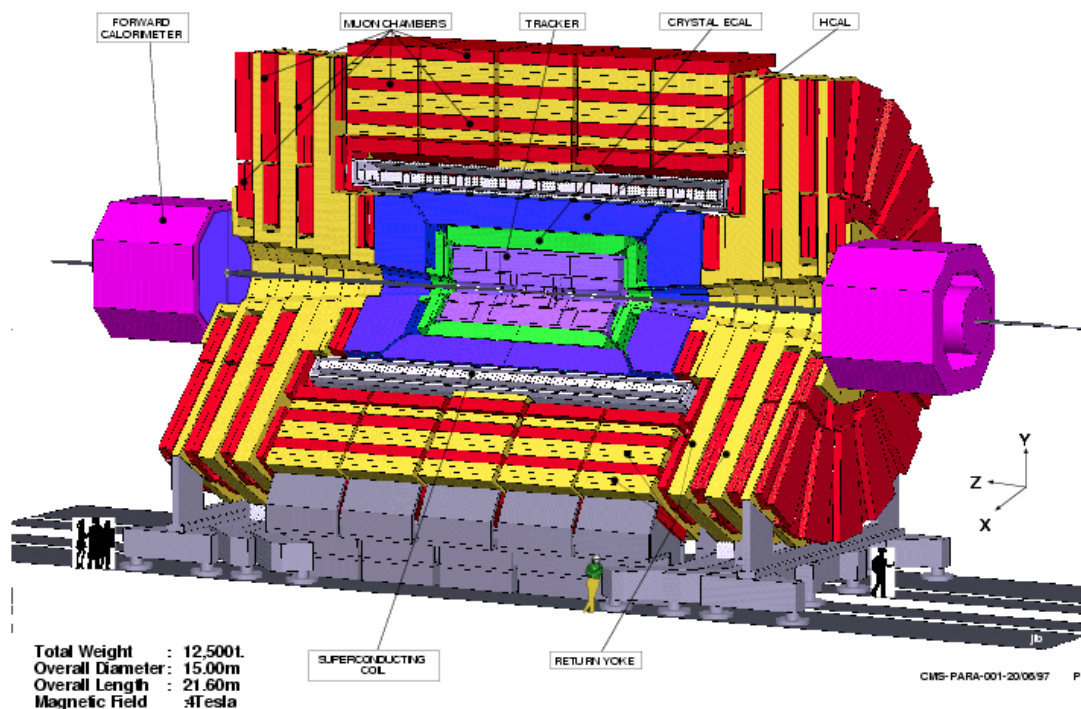


Figure 1: Overview of the CMS experiment.

## 2 The CMS experiment

CMS will be the other of the two big general purpose experiments at the Large Hadron Collider (LHC). The LHC will collide two proton beams head-on at a center of mass energy of  $\sqrt{s}=14$  TeV and a luminosity of  $10^{34} \text{ cm}^{-2}\text{s}^{-1}$ . It is expected that at peak luminosity about  $8 \times 10^8$  collisions are produced per second. Each of these will deposit about 5 TeV of energy in the experimental area while the remaining 9 TeV will be distributed in the LHC machine.

The layout of the CMS experiment, shown in Fig. 1, is very classical. The detectors are grouped around a large superconducting magnet, which provides a solenoidal field of 4 T over 14 m of length and 6 m diameter. At the center of the detector the Inner Tracker is used to exactly measure the momentum of charged particle tracks via their curvature in the magnetic field. The Tracker has to be as light as possible in order not to intercept the particles. Next comes an electromagnetic calorimeters (ECAL) made of  $\text{PbWO}_4$  crystals. The role of this device is to stop all photons and electrons and to accurately measure their energy. A significant amount of hadronic interactions – and thus activation – take place in the ECAL. After the ECAL a brass/plastic-scintillator hadron calorimeter (HCAL) has the role to intercept all hadrons and measure their energy. Ideally only muons (and practically undetectable particles like neutrinos) will penetrate the HCAL. These muons are detected by the muon spectrometer, which consists of four layers all embedded in the massive steel return yoke of the solenoid.

The central detectors described above cover up to a pseudorapidity of  $\eta=2.4$  (Tracker) or 3.0 (calorimetry). In the very forward regions, between  $\eta=3-5$ , the forward calorimeter (HF) is used to measure the

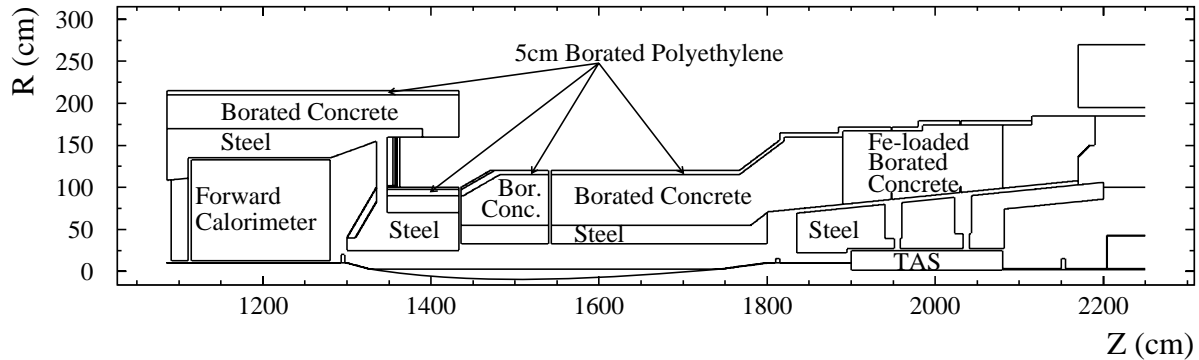


Figure 2: Schematic view of the CMS forward shielding as described in the geometry files of the radiation simulation code.

$E_\gamma$ (keV)	Concrete	Aluminium	Iron	Lead
500	4.89	4.37	1.54	0.59
1000	6.68	6.04	2.14	1.29
2000	9.52	8.57	3.0	1.95

Table 1: Narrow beam mean free paths (in cm) in some common shielding materials.

energy of both the electromagnetic and hadronic sector. In this region the highest activation levels are expected.

Even further forward, at  $\eta > 5$ , there are no detectors in the high-luminosity configuration of CMS. But the forward beam-line is hit by the secondary particles emerging from the interaction point (IP) and heavy shielding is required in order to reduce the background in the experiment. The shielding around the forward beam-line is shown in Fig. 2. An especially intense source of background is the TAS absorber at the end of the experimental cavern. The main function of this element is to protect the superconducting quadrupoles of the focusing triplet from the heat load due to the particles from the IP. Since the TAS absorbs a large amount of energetic hadrons, it will feature correspondingly high induced radioactivity levels.

### 3 Shielding materials

The dose due to induced activity is usually caused by photons, which are emitted in the decay of radioactive nuclei. Most radionuclides exhibit  $\beta$ -decay, in which case an electron or a positron are emitted. These have only a very limited range in matter, so they are significant only for thin objects, where the accompanying dose due to the more penetrating photons remains small. The  $\gamma$ -dose always dominates the whole-body exposure and in these studies only that component will be considered.

The energy of the photons varies from soft X-rays to an upper limit of about 10 MeV. For nuclides which

are stable on a macroscopic time scale, i.e. at least several minutes, photons above 3 MeV are very rare. The soft photons cause mostly only surface effects, i.e. they are quickly absorbed by thin shielding and the self-attenuation in the active medium is significant. With increasing photon energy the penetration depth in shielding material increases and therefore photons above few hundred keV start to become really significant. The narrow-beam mean free paths for some energies and materials are listed in Table 1. The narrow-beam values refer to the attenuation of a monoenergetic collimated beam, i.e. each particle scattered out of the beam or down in energy is counted as attenuation. Thus these values provide the most optimistic limit for shielding applications, because the scattered particles can still contribute to the dose. This effect is called build-up and depends on the attenuating medium and the initial photon energy. The build-up changes the slope significantly only at small penetration depths. After several attenuation lengths the primary photon flux and the build-up contribution are in equilibrium and the dose attenuation follows rather well the narrow-beam mean free path. Fig. 3 shows a FLUKA [2] simulation of the dose attenuation in Lead, and an analytical attenuation curve. It should be noted that the FLUKA simulation is done for a large plane source – a representative case for active elements in CMS – emitting photons along the z-axis, whereas the build-up factors in the analytical curve are for an isotropic point source. This probably accounts for the difference.

Actually 1 MeV, used to produce Fig. 3, is probably an overestimate for the average photon energy. In real cases the spectrum will comprise a few  $\gamma$ -lines above 1 MeV, but a larger number below. In steel, activated by high-energy hadrons, the most significant isotope is usually  $^{54}\text{Mn}$ <sup>3</sup>, which has a single  $\gamma$ -line at 0.835 MeV. Thus the dose from steel is somewhat stronger attenuated by Lead than Fig. 3 would indicate.

Fig. 3 shows that at 1 MeV of photon energy Lead is almost exactly twice as good a shielding material as Iron in terms of thickness. Even in the attenuation per unit weight comparison Lead remains superior to Iron. Towards lower energies the superiority of Lead increases, whereas the material dependence slowly diminishes at higher energies.

## 4 Simulation procedures

The hadron cascade simulations for CMS are performed with with FLUKA and yield the star densities<sup>4</sup> in the various detector and shielding elements. These star densities could be used with the newly evaluated  $\omega$ -factors [3]. However, these were evaluated only for a few characteristic spectra. For better accuracy the activities and emitted  $\gamma$ -spectra have been re-evaluated for the various CMS sub-detectors with the proper spectra. In most situations the difference to the  $\omega$ -factors from [3] is likely to be small, but for some cases with a very peculiar spectrum – like for instance the beam-pipe – the difference can be more significant. The computational procedure is in principle the same as outlined in [3], i.e. residual nuclides are scored with FLUKA and their time evolution and energy emission is followed with the DeTra[4] code. The low-energy neutron activation was combined with the high-energy activation and everything was scaled to the star density. This is a valid and accurate procedure only because the same spectrum which generates the stars is used also in the activation analysis so that the ratio of low-energy neutrons to stars is the same in both cases. In large bulk objects like calorimeters the residual nuclide scoring is done within a representative region directly in the full CMS simulation. In thin objects like the beam pipe such a procedure would not yield sufficient statistics. In these cases a representative spectrum is

<sup>3</sup>For a given material the relative importance of isotopes depends mainly on the cooling time and to a lesser extent on the irradiation time.

<sup>4</sup>A star is an inelastic interaction above a given energy threshold for the incident particle – typically 20 or 50 MeV. The star density is fairly well proportional to induced radioactivity per unit volume.

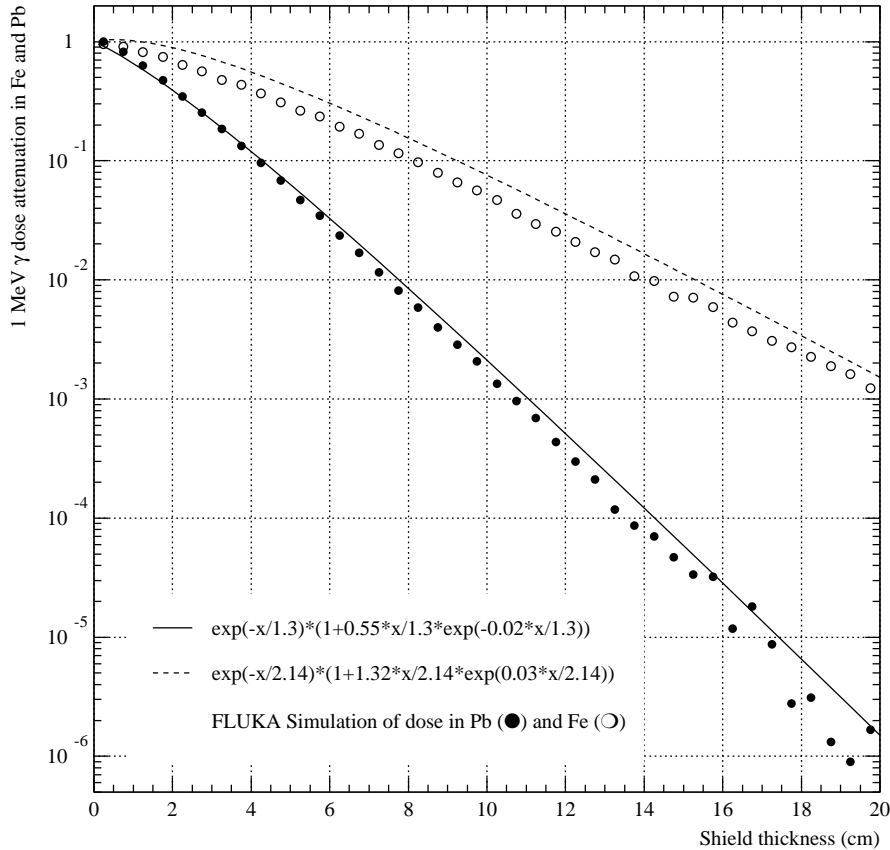


Figure 3: Attenuation of dose due to 1 MeV photons as a function of Iron and Lead thickness. In the simulations the dose is that in Fe (or Pb) and the total shielding thickness was 30 cm.

used in a second simulation to estimate the radionuclide yields.

From the residual nuclides predicted by the FLUKA/DeTra calculation the exact distribution of  $\gamma$ -lines was determined. For computational simplicity the spectrum was then collapsed into 7 generic lines with energies of 200, 350, 500, 700, 1000, 2000 and 4000 keV. In this procedure the intensities of the lines were adjusted so that energy was conserved. These seven lines were then used by the FIASCO [5] code to calculate the dose rates close to the activated bulk objects. FIASCO uses the FLUKA geometry and information about photon attenuation and buildup to integrate the dose from the whole activated object. The analytical attenuation curves shown in Fig. 3 correspond to those used in FIASCO.

## 5 Benchmarking the simulations

The prediction of the residual nuclide yield by a Monte Carlo simulation is just as good as the physics model implemented in the simulation. Typically the models used in high-energy hadronic codes are intended to reproduce the development of the hadronic cascade and therefore emphasis is put on the production of fast secondaries. The residual nucleus is, indeed, often just a left-over of the reaction as described in the model. If, however, the model is based on sound physics foundations, this leftover also should correspond rather well to reality. For the models in the FLUKA code, there is good reason to believe that the residual nuclide distributions would be rather well reproduced. In order to verify this, we irradiated small samples of Aluminium, Iron, Copper and Lead in the IRRAD2 facility at the CERN PS

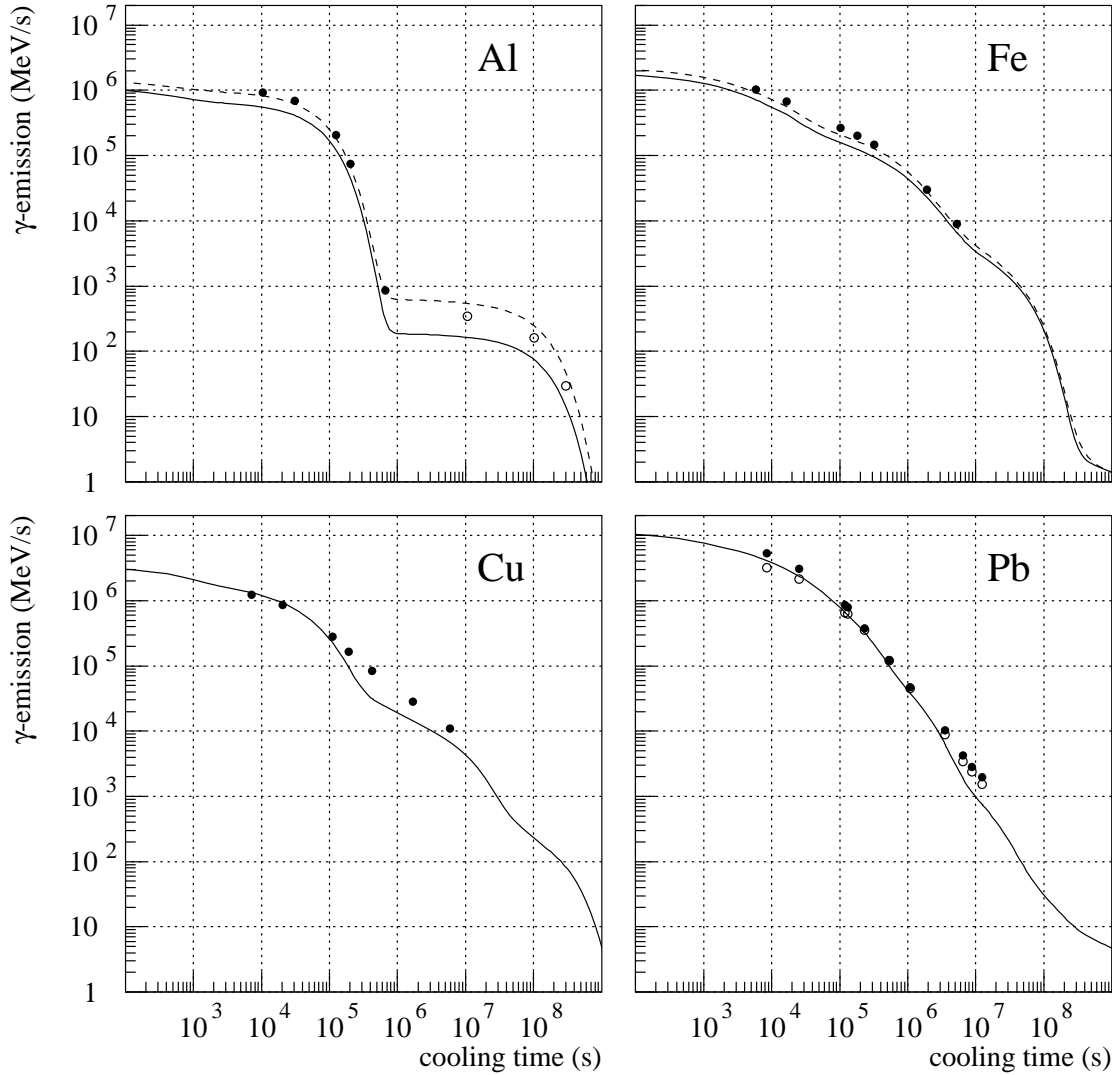


Figure 4: Comparison of calculated (lines) and experimental (dots) total gamma energy emissions from the samples. The solid line shows the FLUKA residual nuclide calculation and the dashed the same complemented with experimental cross section data. The open dots in the Al-comparison show the dose due to  $\text{Na}^{22}$  calculated from the activity of the last measurement (solid dots). In the Al, Fe and Cu plots the experimental values are based on the photo-peak information. In the Pb-plot the solid dots show the energy from integrating the whole spectrum while the open dots show the dose derived from the photo-peaks found in the spectrum [6].

accelerator. This facility produces a particle spectrum which resembles rather well that expected in the CMS calorimeters – including a high-energy component of charged hadrons and fast neutrons, but also a significant flux of neutrons below 20 MeV. Details of this study are reported in [6]. In Fig. 4 the main results are summarised as a comparison of the FLUKA prediction of the total emitted energy in form of photons and the value measured with a HPGe-detector.

For Aluminium we can observe some discrepancies due to the fact that only one radionuclide at a time dominates the dose –  $\text{Na}^{24}$  at short cooling times and  $\text{Na}^{22}$  thereafter. Any error in the yield of these nuclides is directly reflected in the total dose estimate. It should be pointed out that the absolute scale of the plots is determined by the flux calibration of the irradiation, which was performed by fitting the

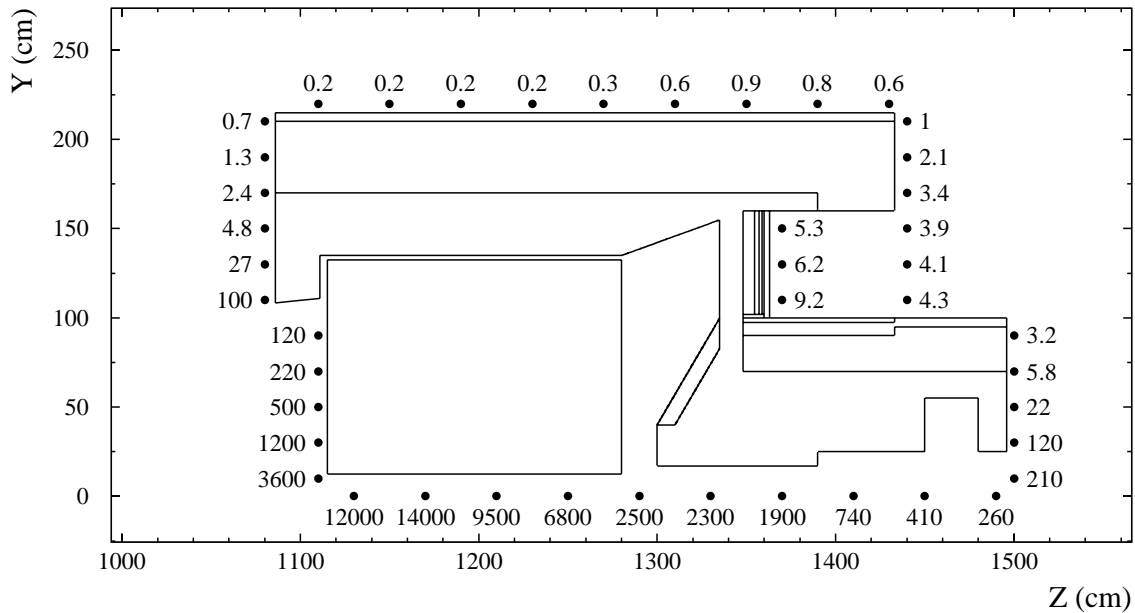


Figure 5: Induced radioactivity levels around the HF after 10 years of LHC operation and 1 day of cooling. These are based on a FLUKA/DeTra prediction of radionuclide yields and a dose integral performed with FIASCO.

measured  $\text{Na}^{24}$  activity to the calculation (using available experimental cross sections).

In the case of Iron several nuclides start to contribute and errors in opposite directions on individual nuclides start to cancel each other in the total dose. It should be said, however, that the most important nuclides with respect to the dose are very accurately predicted in Iron.

In Copper a discrepancy is observed at intermediate cooling times. This could be traced back to three nuclides which give a significant contribution in this time range and are all underestimated by a factor of 2–4.

In the case of Lead, especially for short cooling times, statistics works fine and in the huge amount of radionuclides none is able to dominate over another and errors average out very well. Towards longer cooling times the number of nuclides decreases and some discrepancies start to appear. It must be said, however, that here the measurements start to suffer from natural background which we have not yet removed from the dose analysis.

Detailed comparisons at the level of individual nuclides can be found in [6].

## 6 Shielding of the HF calorimeter

The Forward Calorimeter (HF) will become the most radioactive sub-detector of CMS. Close to its front face induced activity dose rates of few mSv/h are expected locally. In order to provide safe working conditions in the vicinity of the garage where the HF is stored during maintenance periods, dedicated shielding, which covers the most active parts of the detector, has to be designed.

Setup	2 cm Fe	2 cm Pb	4 cm Pb	6 cm Pb	8 cm Pb	Pb mass in t (door/curtain)
-1	—	—	—	—	—	0/0
0	0–220	—	—	—	—	0/0
1	0–220	—	—	0–100	—	0.7/1.4
2	0–220	—	50–100	0–50	—	1.6/0.8
3	0–220	100–150	—	0–100	—	1.6/1.4
4	0–220	100–150	30–100	0–30	—	1.6/0.8
7	0–220	50–150	30–50	0–30	—	1.6/0.24
8	0–220	120–150	50–120	—	0–50	1.6/1.4
9	0–220	110–150	70–110	—	0–70	1.6/1.6
10	0–220	110–150	80–110	30–80	0–30	1.6/1.4
11	0–220	0–150	—	—	—	1.6/0
12	—	80–110	30–80	0–30	—	0/1.4

Table 2: Radii of the shielding disks of the HF garage doors and the curtain fixed on the HF.

The design limit for the dose in controlled radiation areas is  $10 \mu\text{Sv/h}$ . With a  $5 \text{ mSv}$  annual limit this would allow an occupancy time of 500 hours, corresponding to 62 shifts of 8 hours. For all practical cases this should be sufficient. However, there are a few arguments to justify that the shielding in front of the HF should be lowered to the level of  $1 \mu\text{Sv/h}$ :

- In order to fully obey the ALARA principle the HF shielding should be designed – if reasonably achievable – to give the same dose-rate as in the surrounding cavern, which is about  $1 \mu\text{Sv/h}$  or slightly below.
- The induced activity predictions have non-negligible uncertainties and a safety factor of about 5 should be foreseen – in particular since the dose rates predicted by our more detailed FLUKA/DeTra calculation are about a factor of about 3 lower than formerly used  $\omega$ -factors [7] (which thus could be considered to have implicitly included a safety factor of 3).

For these reasons we have set the target that the shielding of the HF and of the garage doors should yield a dose rate of  $1 \mu\text{Sv/h}$  outside of the HF garage.

From Fig. 5 it can be seen that the dose rates are highest close to the front high- $\eta$  corner of the HF, but they exceed the  $1 \mu\text{Sv/h}$  level over almost the entire front face up to the outer periphery of the lateral shielding. In case the HF is not positioned very close to the garage doors, we also have to ensure that enough of the solid angle is covered by the shielding on the doors. Therefore we propose to have for the shielding on the doors the same radius as for the lateral shielding of the HF itself.

It has been decided to split the HF shielding into two components. The first is a *curtain* which is supported on rails on the permanent HF lateral shielding, is open during beam operation but can be slid in front of the HF absorber before the latter is retracted from the CMS end-cap. This curtain will cover only the active absorber of the HF. It will lower the dose in the HF surroundings and thus the safety precautions during the transfer into the garage are more relaxed.

When the HF is in the garage the doors of the latter will be normally closed. These doors are a lightweight steel structure, but incorporate a 2 cm steel plate and additional Lead shielding. The steel plate will cover

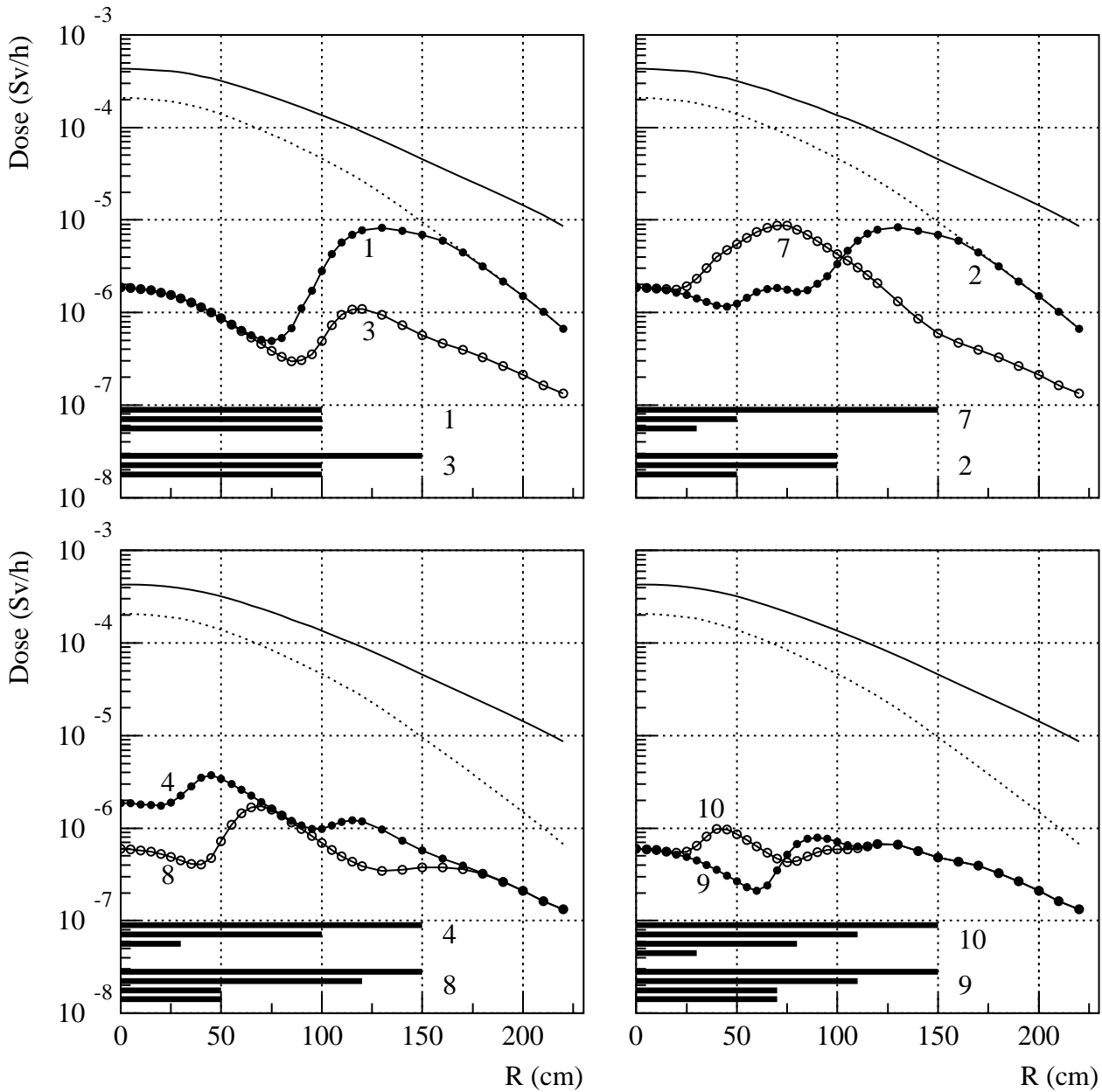


Figure 6: Dose in front of the HF for various shielding configurations. The solid line shows the case of no shielding and the dotted line corresponds to only having a 2 cm thick steel plate with radius 220 cm. The black lines on the bottom of each plot show the radial extent of the Lead plates for each configuration. The exact radii are given in Table 2

the entire HF front face up to the outer periphery of the lateral shielding while the extent of the Lead plate can be slightly reduced to match the radial dependence of the activation. Fig. 6 shows an optimization study of the Lead thicknesses in these two shields.

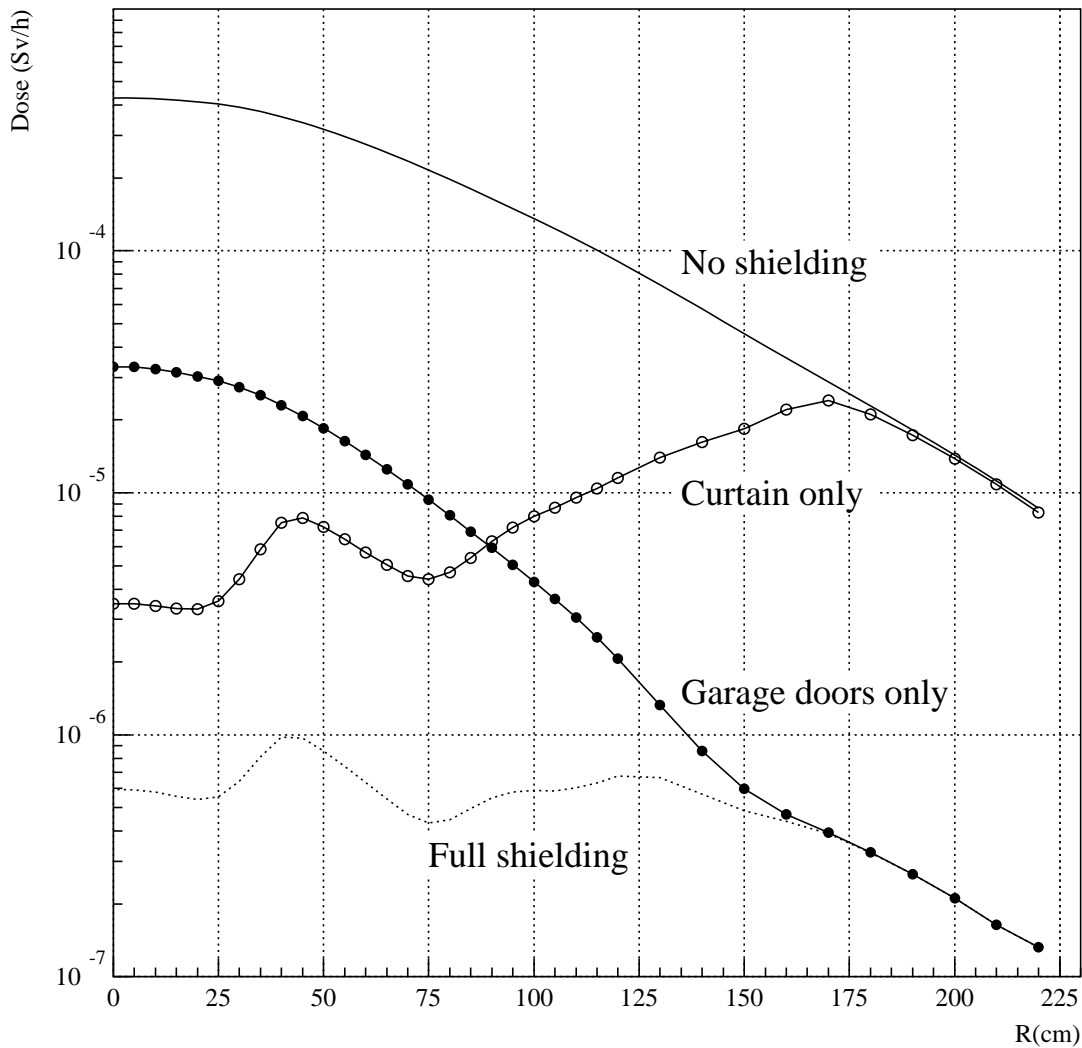


Figure 7: Dose in front of the HF for no shielding at all (solid line), for the full shielding configuration 10 (from Table 2) and for having only the garage doors or only the 'curtain' of the HF closed.

The exact radial ranges of the shielding plates in the optimisation study are given in Table 2. The 2 cm Fe-plate is always in the garage door. Each of the Lead plates is assumed to be 2 cm thick and the first plate is fixed on the steel plate of the garage door. The radial ranges are given as cumulative values, i.e. the upper limit of the 2 cm column gives the upper limit of the first Lead plate (on the door), the 4 cm column the upper limit of the second Lead plate (on the curtain), etc. Each plate starts at  $R=0$ .

One of the quantities to take into account is the total mass of the Lead on the door and on the curtain. Obviously this should be minimized while keeping the desired shielding performance. Fig. 6 indicates that configurations 9 and 10 both meet the  $1 \mu\text{Sv/h}$  design goal. Since configuration 10 has a smaller mass of Lead on the curtain, this is our preferred solution. Thus the garage doors will comprise a 2 cm steel plate up to  $R=220$  cm equipped with one 2 cm Lead plate up to  $R=150$  cm.

The curtain on the HF will consist of a stack of three 2 cm thick Lead plates, with radii of 110 cm, 80 cm and 30 cm. All these plates, both on the door and the curtain are centered on the HF axis.

Fig. 7 shows the dose in front of the HF when only the curtain is closed (transfer to garage) or when

the doors are closed and the curtain is open (unlikely situation, but could happen in garage position). In both cases the controlled area design limit is only slightly exceeded. Since these configurations concern special situations even a significant excess could be justified. This good performance of either shielding component alone is an additional asset for the design.

Fig. 8 shows the time evolution in the radioactivity in the steel of the high- $\eta$  front corner of the HF. It is assumed that the luminosity of the LHC increases gradually over the first three years, such that it is  $10^{33} \text{ cm}^{-2}\text{s}^{-1}$  in the first year,  $3.3 \times 10^{33} \text{ cm}^{-2}\text{s}^{-1}$  in the second year and  $6.7 \times 10^{33} \text{ cm}^{-2}\text{s}^{-1}$  in the third year. From the fourth year onwards  $10^{34} \text{ cm}^{-2}\text{s}^{-1}$  are assumed. Furthermore each year of operation is assumed to consist of three running periods of 60 days each, interleaved by 14 day short stops. Neglecting the heavy-ion operation, this leaves a long annual shutdown of 157 days. It has been estimated [8] that for each day of operation the average luminosity is about half of the peak value at the start of a fill. The vertical scale in Fig. 8 is defined in a way which implicitly includes these definitions. The star density is normally extracted from simulations for peak luminosity. Thus the curve is scaled to give the amount of energy emitted in form of gamma rays per second normalized to the production rate of stars (per second) at LHC peak luminosity. Due to this definition the quantity shown in Fig. 8 is not directly related to the commonly used concept of  $\omega$ -factor [3].

The main conclusions to be drawn from Fig. 8 are, however,

- the induced activity dose is almost exactly proportional to the luminosity, i.e. there is very little slow buildup. Thus the activity after the first year at high luminosity is essentially the same as after any further year,
- the dose does not decrease significantly between 1 day of cooling and 7 days of cooling,
- the dose decreases only by a factor of 3.5 between 1 day of cooling and the end of an annual shutdown (157 days of cooling).

Although these results are obtained for Iron, the time dependence is rather similar for most materials above the Iron mass (see Fig. 4). Thus Fig. 8 gives an indication how the dose rate will evolve as a function of time for all the cases discussed in this note.

## 7 Dose rates around end-cap calorimeters EE and HE

To estimate the dose rate during maintenance, the relevant configuration of CMS is the 10 m opening. In this case the HF is in the garage and the end-cap calorimeters are retracted from the barrel detector. Thus only the dose rate due to activity in the end-cap itself is relevant.

Fig. 9 shows the dose rates in the vicinity of the end-cap calorimeters. It can be seen that typically doses of about  $500 \mu\text{Sv/h}$  are reached close to the high- $\eta$  corners. The dose along the  $\eta=3$  boundary gradually decreases as a function of depth in the HE.

More important, however, is the dose as a function of distance from the front face of the EE. The design limit of  $10 \mu\text{Sv/h}$  is reached at a distance of 2–3 metres from the EE face.

For the estimates in Fig. 9 the preshower has been ignored. Being a structure consisting of several thin layers it does not suit the method of dose calculation performed here. The Lead of the preshower would attenuate the dose from the EE – as it does in reality – but its own contribution to the dose would not be correctly predicted because FIASCO is not able to treat thin activated layers. Since Lead has similar

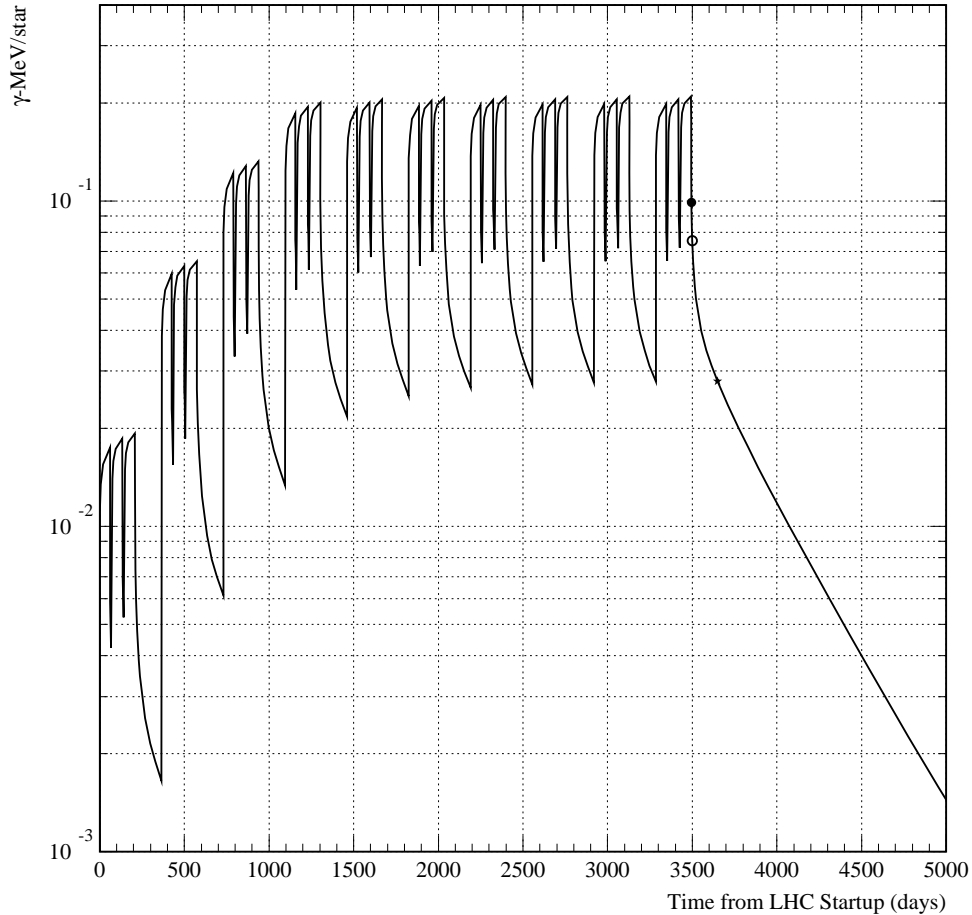


Figure 8: Time evolution of induced activity in the front high- $\eta$  corner of the HF. The first 3 years are with reduced relative luminosities of 10%, 33% and 67%. The solid dot shows the point corresponding to values in Fig. 5, i.e. 1 day of cooling. The open dot and the star correspond to 7 days and 157 days of cooling, respectively. See the text for a discussion of the vertical scale.

activation characteristics as the ECAL crystals, the attenuation of the preshower is likely to be roughly compensated by its own activity and therefore the results presented here should be equally valid for the full EE/preshower assembly.

Most of the foreseen maintenance work on the EE would take place on the outer periphery, where dose rates are of the order of  $10\text{--}50\ \mu\text{Sv/h}$ . Every effort is made to minimize the need of access to the high- $\eta$  corner, where dose rates up to  $500\ \mu\text{Sv/h}$  are predicted. If considered necessary, dedicated temporary Lead shielding similar to that of the HF can be installed in this region. However, detailed design of this shielding is awaiting the exact specification of all foreseen maintenance operations.

## 8 Dose rates in the $\eta=3$ cone

For maintenance of the endcap muon chambers the forward disks will be separated from each other. This will provide access to the vicinity of essentially any position of the forward  $\eta=3$  cone. Fig. 10 shows the expected dose rates due to induced radioactivity within this cone and in the high- $\eta$  region of the endcap muon chamber slots. The chambers themselves are not included in the estimate. The

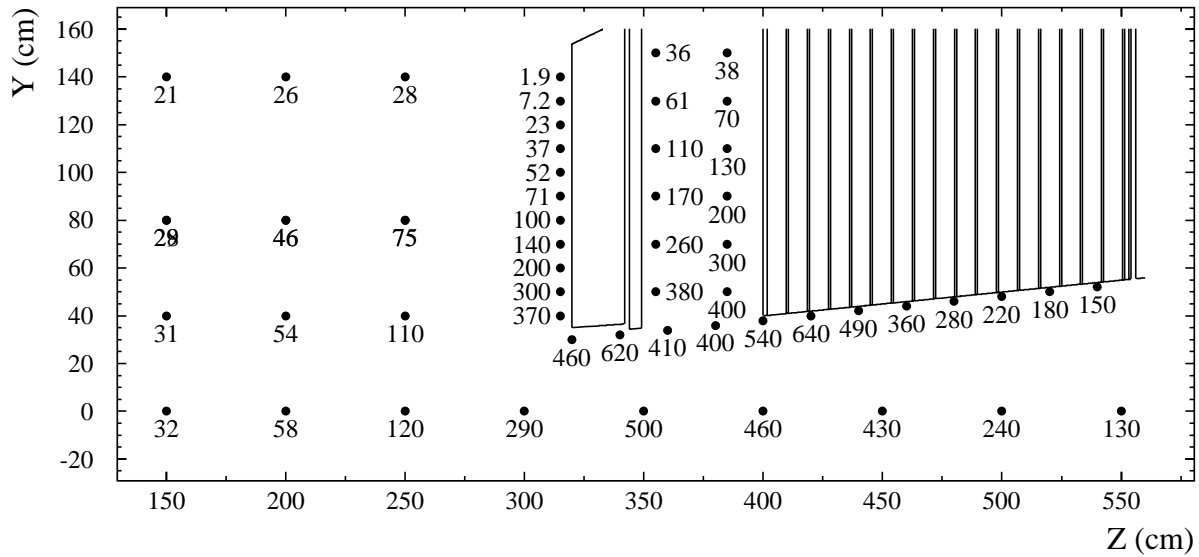


Figure 9: Dose rates ( $\mu\text{Sv/h}$ ) due to induced radioactivity in the end-cap calorimeters. The EE (Electromagnetic End-cap) is located between  $z=320\text{--}342$  cm and the HE (Hadronic End-cap) starts at  $z=400$  cm. The barrel calorimeters are ignored. Therefore the doses correspond to the 10 m opening for maintenance. The values correspond to 10 years of LHC and one day of cooling.

geometrical configuration shown in Fig. 10 does not correspond to the normal maintenance configuration with separated endcap disks. Within the cone the values in Fig. 10 provide an upper estimate with respect to separated disks, while the low values in the chamber slots would increase when the more active surface inside the cone becomes “visible” due to pening up crack between the disks.

It can be seen that – with the exception of ME1 – the dose rates in the region of the end-cap muon chambers are close to the design limit without any shielding. Since these values are for a very short cooling time of only 1 day, no radiation problems are expected during the maintenance of the end-cap muon chambers. However, these values do not include the activity due to the beam pipe, which might be left in place during maintenance.

With the disks closed the dose values within the chambers slots are only about an order of magnitude above natural level in the Geneva area. This means that the yoke at  $\eta < 2.5$  has very low remnant radioactivity even after 10 years of operation and only 1 day of cooling.

## 9 Dose rates around the TAS region

The TAS has an inner bore of  $R=17$  mm, covers up to a pseudorapidity of  $\eta=7.8$  and thus absorbs about 2 TeV of energy per pp-event. In comparison, each of the forward calorimeters (HF) absorbs about 300 GeV per event. Since in an environment dominated by hadron irradiation, the induced activity is roughly proportional to the absorbed energy, the TAS will be by far the most radioactive element in the CMS area.

For this reason the TAS in CMS has been embedded inside an Iron shield, called the Fixed Iron Nose (FIN). The design criteria were such that the FIN fits into the  $\eta=3$  cone of CMS when the end-caps are

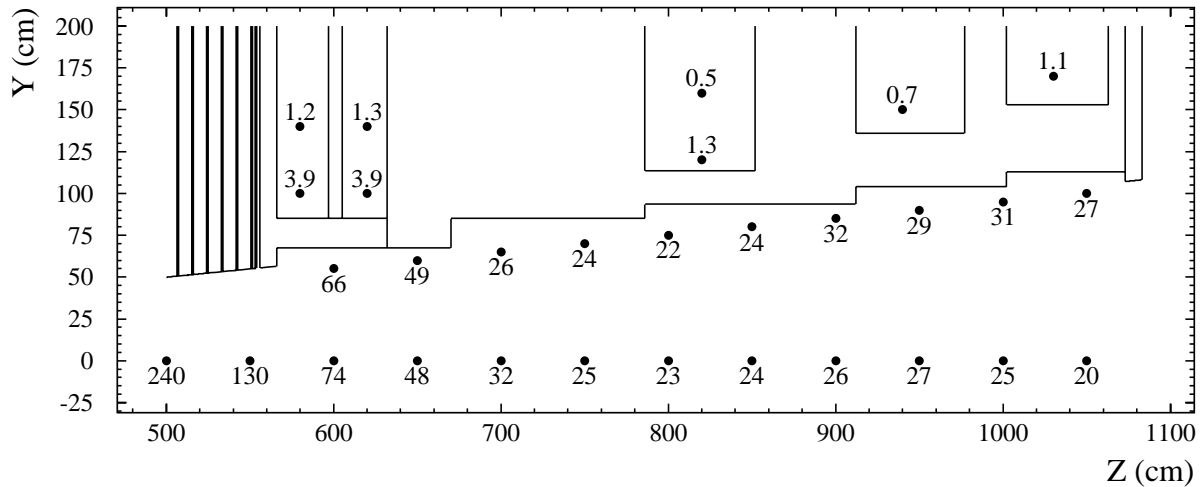


Figure 10: Dose rates ( $\mu\text{Sv/h}$ ) due to induced radioactivity in the high- $\eta$  parts of the end-cap disks. The HF is assumed to be removed to its garage. The values correspond to 10 years of LHC and one day of cooling.

retracted by 10 m, but also that in normal conditions the FIN prevents access to the immediate vicinity of the TAS. Thus the TAS itself will be accessed only in the very special – and possibly never occurring – situation that repairs or modifications on it have to be undertaken.

In front of the FIN the main vacuum pump of the experimental region is housed. This pump is likely to need fairly regular access for maintenance. As can be seen from Fig. 11, the dose rates in the front of the FIN at the location of the pump are of the order of 1 mSv/h. The pump itself will be positioned at a radius of more than 22 cm, so that it is protected by the edge of the FIN against neutron albedo from the TAS and by the HF against particles from the IP. These measures significantly reduce the activation of the pump itself. Despite these measures dose rates still will remain high – about 1 mSv/h contact dose rate instead of  $\sim 10$  mSv/h if the pump were positioned on the beam-line.

## 10 Dose rates around the rotating shielding

The forward beam-line ( $z=14\text{--}18$  m) in the CMS area is covered by the rotating shielding, which attenuates the particle flux emerging from the back of the HF, the TAS and interactions of fast secondaries with the beam-pipe in that region. This shielding will be folded back on top of the platform and the end of the cavern to clear the space for retracting the CMS end-caps.

In the normal operating position only the outer surface of the rotating shielding will be accessible. Fig. 12 shows that expected doses on this outer surface remain at the level of  $1 \mu\text{Sv/h}$  or less.

When the shielding is folded back on the platform, the most active inner Iron shell of the thin part will face the block-house wall and thus it will normally not be accessible. The inner surface of the thick part, however, will remain openly visible towards the cavern. According to Fig. 12 the dose rates expected are of the order of  $50 \mu\text{Sv/h}$ . It should be taken into account, however, that these rates are obtained inside the

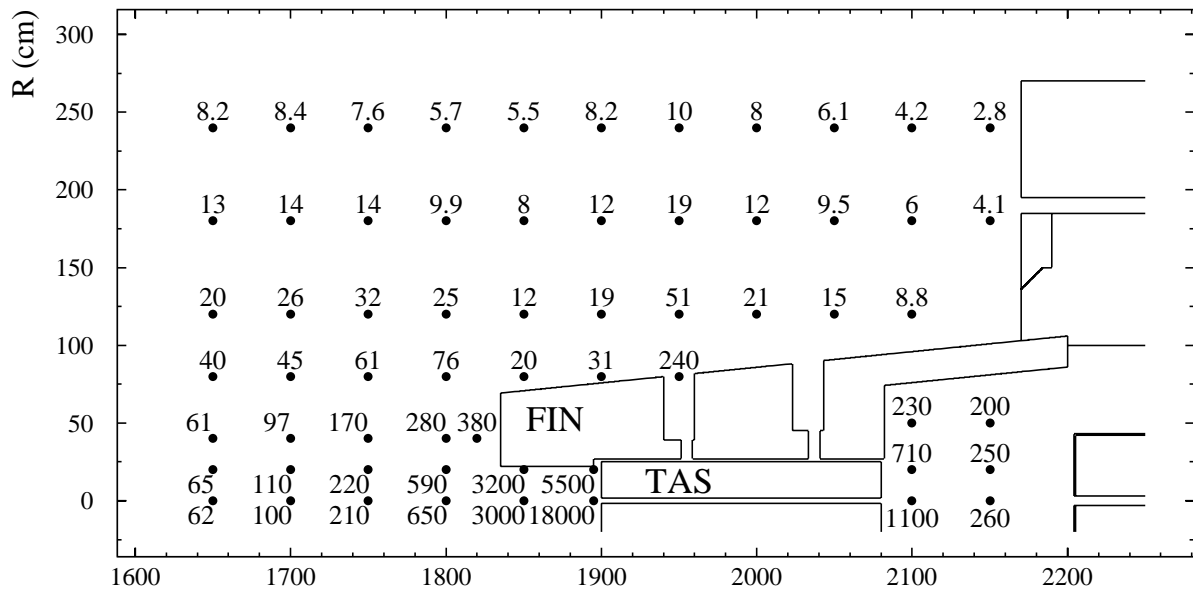


Figure 11: Dose rates ( $\mu\text{Sv/h}$ ) due to induced radioactivity around the TAS and the Fixed Front Nose. Values are after 10 years of operation and 1 day of cooling. The beam-pipe elements are not included in the estimate.

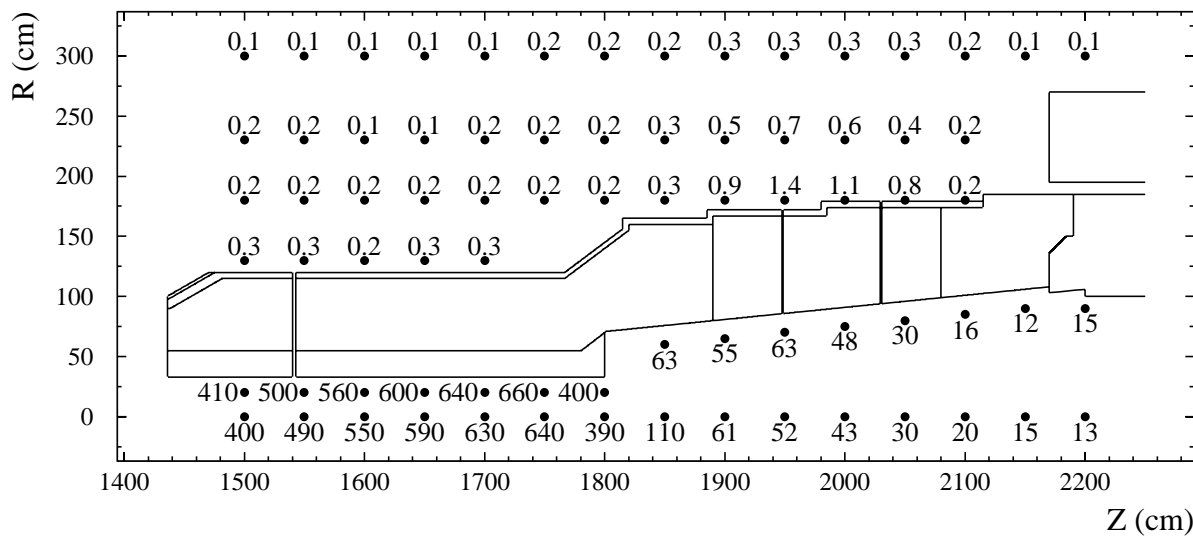


Figure 12: Dose rates ( $\mu\text{Sv/h}$ ) due to induced radioactivity around the rotating shielding. Values are after 10 years of operation and 1 day of cooling. The beam-pipe elements are not included in the estimate.

closed shielding, i.e. inside a closed cavity. In the case of the opened shielding, only one half-shell will contribute. The visible active surface increases somewhat in this case, so the values will not be exactly half of those in Fig. 12, but certainly Fig. 12 represents the upper estimate with respect to the opened shielding.

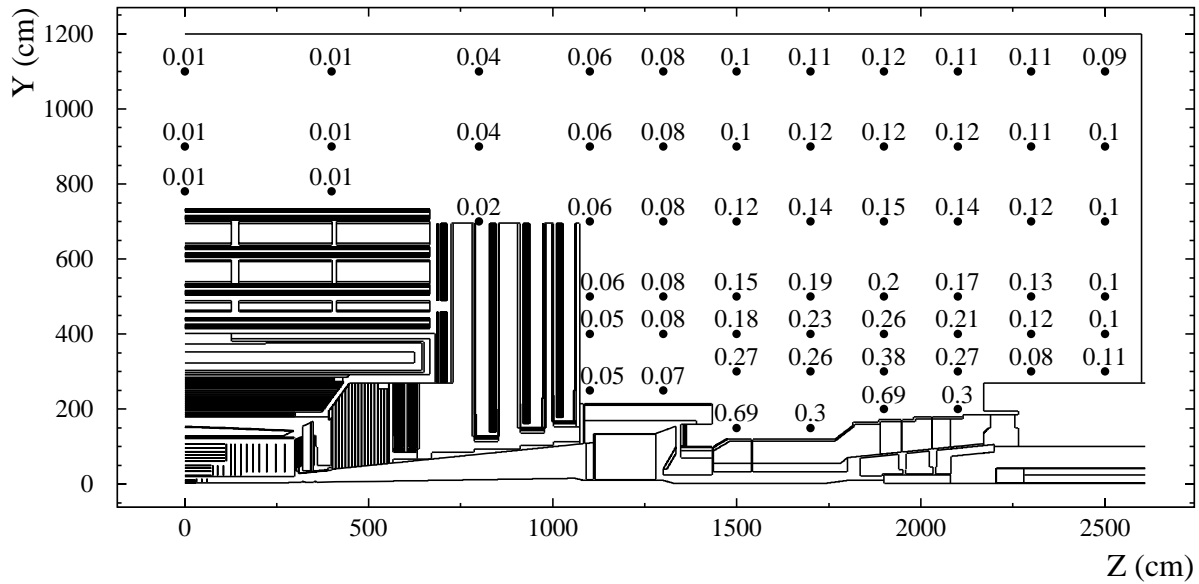


Figure 13: Dose rates ( $\mu\text{Sv/h}$ ) due to induced radioactivity in the CMS experimental cavern (UXC) with the CMS detector and forward shielding closed. Values are after 10 years of operation and 1 day of cooling.

## 11 Dose rates in the UXC

Fig. 13 shows the dose rates expected in the UXC cavern when the CMS detector and the forward shielding are closed. It can be seen that values do not exceed  $1 \mu\text{Sv/h}$  anywhere in the cavern. Thus no access restrictions to the UXC due to induced radioactivity are expected. Especially alongside the cavern walls and the CMS Yoke, where balconies with electronics racks will be located, the dose rates are roughly at natural level. This means that access to the electronics even during short machine stops will not be prevented by radiation levels.

It should be specially emphasised that the outer shell of the CMS forward shielding will be made with borated concrete ( $>0.5\%$  Boron by weight). This Boron content ensures that thermal neutron activation of possible trace elements in the concrete, like Sodium or Eurobium, will be quite efficiently suppressed.

## 12 Dose rates around the beam-pipe

The beam-pipe is a special case, quite different from those discussed before. In contrast to calorimeters and shielding, it is a lightweight structure located in the most intense radiation environment. The hadronic interactions are mostly due to high-energy hadrons and neutron activation plays a relatively minor role.

The induced radioactivity has been estimated by calculating the residual nuclide yield as an average over various sections of the beam-pipe, where the radiation characteristics are different. These sections were:

1. the first short conical section between  $z=2-3$  m,
2. the second long conical section between  $z=4-10$  m,

### 3. the cylindrical section inside of the HF.

All these sections are stainless steel. The dose rate from the central beryllium section is assumed to be negligible and has not been considered.

The obtained residual nuclide yields were normalized with the fast hadron fluence in the same section. In this case the use of fluence instead of stars provides far better statistics. The residual nuclide yield inside the HF was used also for the pipe between the HF and the TAS.

In a second step of simulations a fluence map with very high spatial resolution was used together with these renormalized nuclide yields to calculate the  $\gamma$ -energy emitted by any volume unit of the pipe. Finally an integral over the volume of the pipe was taken to arrive at the final dose rate estimates around the pipe.

The values in Fig. 14 indicate the induced activity  $\gamma$ -dose rate at various distances from the pipe after 10 years of irradiation and 1 day of cooling. It is to be emphasized that  $\beta$ -dose rates are not considered. Especially the  $D=5$  mm values would increase due to these by approximately a factor of 2 – but of course only for the skin dose [9].

Typically one could assume that the values at 5 mm and 10 cm from the pipe surface correspond to the dose a person working on the pipe would get on his hands, while the values at 50 cm and 1 m give an indication of the whole-body dose this person would be exposed to when standing next to the pipe.

The probably most interesting value is the dose at  $R=50$  cm from the pipe axis, because it gives the best estimate of the whole body dose to a person working on the pipe. Therefore this value has been plotted in Fig. 15 for cooling times of 1 day, 7 days and 156 days. The latter value corresponds to the end of the annual shutdown in the assumed operation scenario. Thus the first two values give an indication of the dose rate while disassembling the pipe, whereas the last value gives the dose rate during re-installation.

The CMS detector is designed such that during normal maintenance the beam-pipe stays in place, filled by ultra-pure gas to atmospheric pressure and protected by a shell against mechanical accidents. The protective shell will be designed solid enough to be able to locally support Lead plates of a few centimeters thickness. These might be needed for instance when access is required to the end-cap muon system in which case the disks of the CMS end-cap yoke are separated to create an access to the chambers. The beam pipe will reside in the middle of these disks possibly with gangways or access to its vicinity.

The estimates for the beam-pipe activation presented in Figs. 14 and 15 correspond to the CMS high-luminosity beam-pipe. The newly introduced reinforced forward shielding is likely to allow operation with a unique beam pipe suitable also for TOTEM and other forward detectors. This pipe will feature a very thin section in the  $z=15-18$  m region and some additional flanges and a pump station at  $z=13$  m. Pending a detailed design to do a simulation, the effects of these have been roughly estimated and it seems that in total the dose goes slightly down in the 15–18 m region and the introduction of the pump at 13 m (in the shadow of the HF) does not introduce a dramatic spike into the dose rate.

## 13 Dose rates around the inner Tracker

Like the beam-pipe, the inner Tracker is a lightweight object consisting of many thin silicon layers, cooling tubes and printed circuit boards with electronics chips. The support structure is carbon fiber, where activation can be considered negligible.

The activation of the silicon is rather straightforward to predict because experimental cross sections are available for a fairly extended range of particle types and energies. The cooling tubes are either

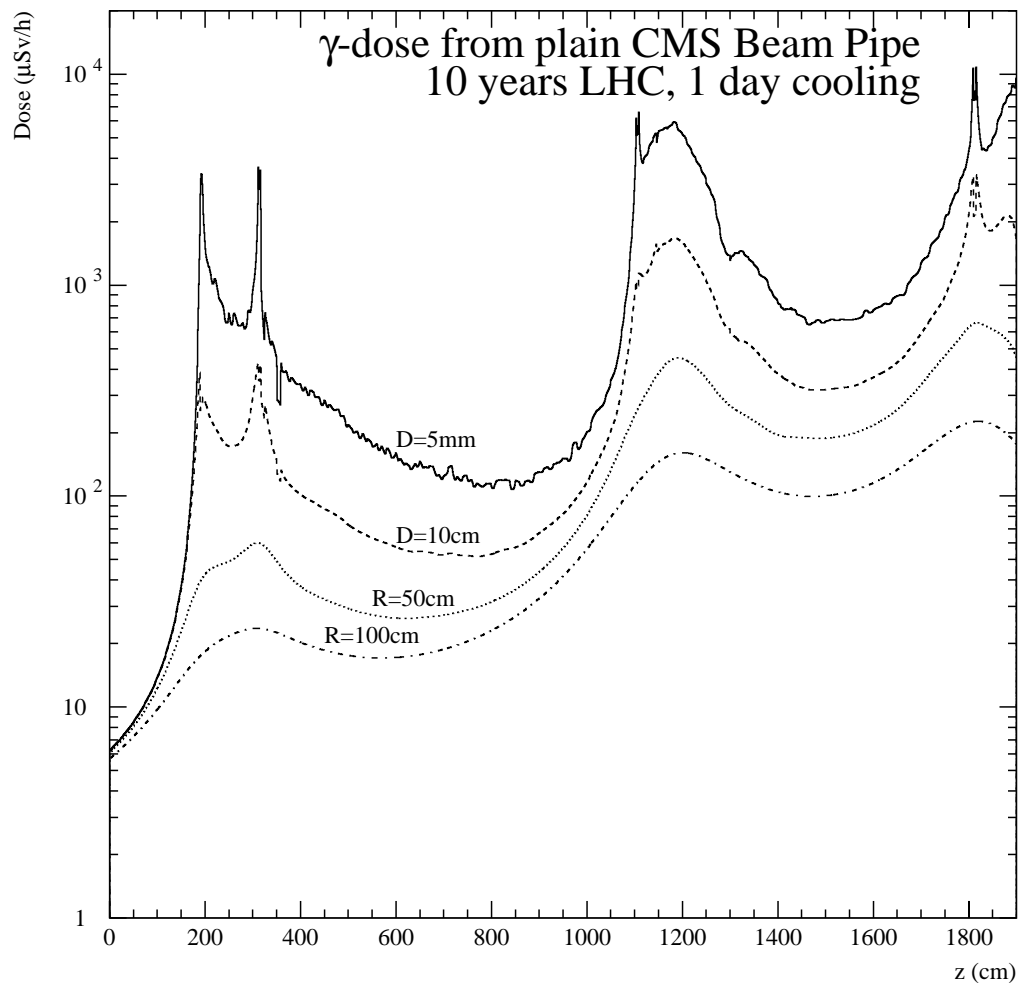


Figure 14: Dose rates around the plain CMS beam pipe. Values are after 10 years of operation and 1 day of cooling. Distances given as “D” indicate the distance to the outer pipe wall and those give as “R” the distance to the center axis of the pipe.

Aluminium in the Pixel and Inner Barrel (TIB), CuNi in the Outer Barrel (TOB) and Titanium in the end-cap (TEC). Also for these, prediction of induced activity can be considered fairly reliable.

The signals from the Tracker are taken out by optical fibers, where activation is negligible. The power cables, however, are either Copper or Aluminium with a thin silver coating to facilitate soldering. This silver – between 3–5 kg in total – is a significant contributor to the total induced activity dose rate in the Tracker.

Most difficult to predict is the dose from the electronics and especially the numerous connectors used in the Tracker. Most of the connectors are collected on the end-flange, which is the only accessible part of the Tracker, unless a Tracker End-caps are removed. Thus any maintenance work on the Tracker will require mainly work in close vicinity of the end-flange where the largest number of components with partly unknown composition is located. Already small amounts of material with high neutron activation (Ag, Au,...) can dramatically change the dose rate estimates in the vicinity of the end-flange.

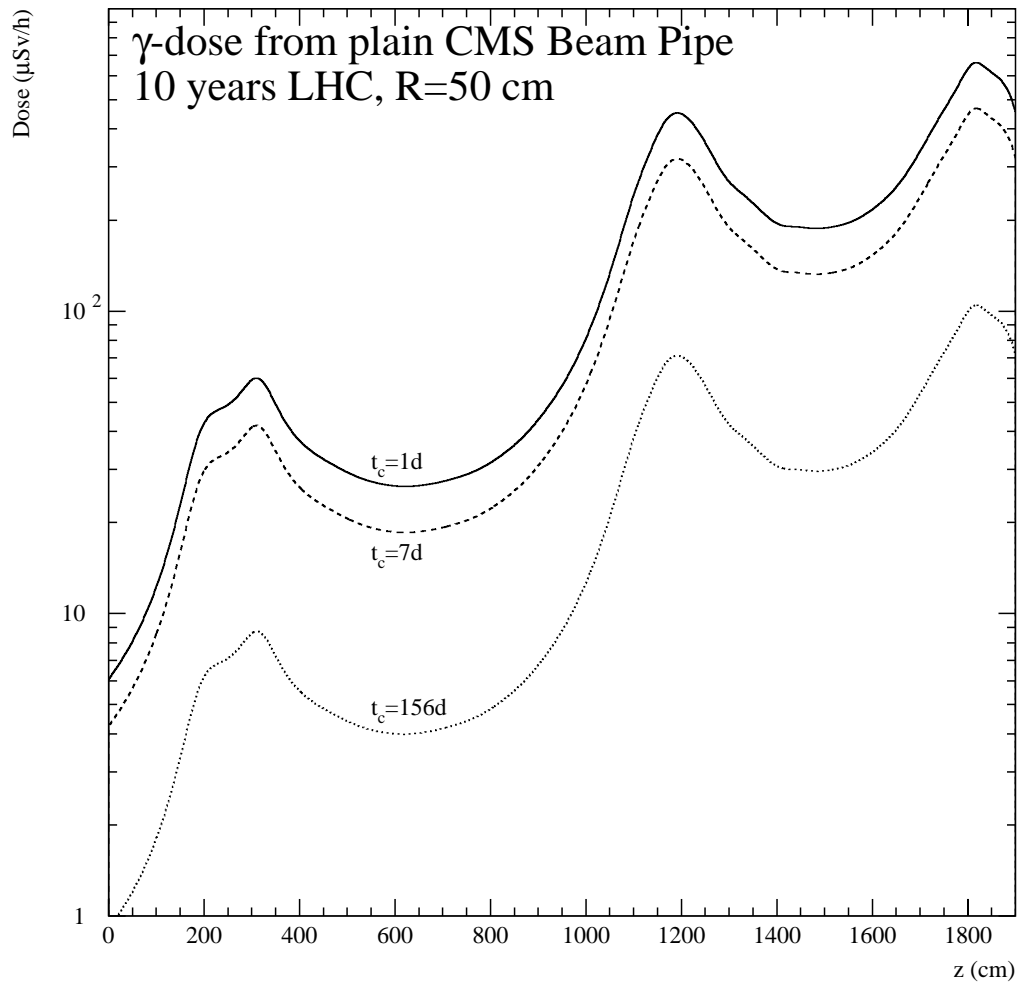


Figure 15: Dose rates around the plain CMS beam pipe at 50 cm distance from the center axis of the pipe. Values are after 10 years of operation and the indicated cooling time.

An extensive study of the activation in the inner Tracker was done for the Tracker TDR [9], but in the five years since the publication of this document there have been some quite significant modifications. Nevertheless, the values in [9] give a fairly good indication of what to expect. A new detailed estimation is motivated only when all cables, connectors and electronics are fully specified.

When the ECAL end-cap is retracted by 5 m or more, it does not contribute to the dose in the Tracker region. Thus the dose comes from the Tracker itself, the ECAL barrel and the beam-pipe, which normally remains in place. Each of these is estimated to contribute about 5–15  $\mu\text{Sv/h}$  (depending on cooling time). The dose from the beam-pipe of course has a rather strong radial dependence. At present we work on the assumption that the average dose rates (over positions and cooling times) at the Tracker end-flange is about 50  $\mu\text{Sv/h}$ . With an annual design limit of 5 mSv, this would allow for a maximum working time of 100 h per person in the vicinity of the end-flange.

Local shielding around the beam-pipe appears feasible. The ECAL barrel represents such a large surface that shielding is not practical. If parts of the Tracker endflange can be shielded while maintenance work

proceeds on other parts, remains to be investigated.

## 14 Conclusions

During its high-luminosity operation the LHC will produce induced radioactivity levels which have never before been encountered in large scale high-energy physics experiments. These activation issues have been anticipated in CMS already at the beginning of the project and procedures and concepts to cope with activation and reduce its impact have been taken into account in the design of the experiment.

The most active part of the CMS experiment itself – the TAS being actually a machine element – is the forward calorimeter (HF). Already at an early stage in the project it was decided that during maintenance of the rest of the detector the HF should be stored in its own garage. In this note a detailed optimisation of the shielding of the HF and of the garage has been given and it is shown that CMS will be able to safely cope with this object, although the dose rates are expected to exceed 1 mSv/h in the most active parts.

Other highly active elements within CMS will be the endcap calorimeters and the beam-pipe, which will normally stay in place during maintenance. While dose rates around these are expected to be about one order of magnitude lower than at the HF, shielding is also more complicated. Temporary shielding, similar to that one described for the HF, can be considered if judged useful, but detailed engineering designs have yet to be worked out. However, the design of these elements had as one aim to minimise the need of access to the most active regions, both in frequency and in duration.

The inner surface of the forward shielding will also show elevated levels of activity, but will not require maintenance and can be stored in a fenced-off location during CMS maintenance.

At the Inner Tracker we expect dose rates of the order of 50  $\mu$ Sv/h and temporary shielding is likely to be difficult. At least no dramatic reduction of rates should be expected. Thus the access time to the vicinity of the Tracker will have to be limited.

When the CMS detector and the forward shielding are closed the dose rates in the experimental cavern (UXC) are predicted to remain below 1  $\mu$ Sv/h after 10 years operation and 1 day cooling. These dose rates do not impose any special access restrictions. Thus access to the UXC to replace electronics modules or for other quick repair work, should be possible even during short machine stops.

All interventions and protection systems will be planned and designed such that the dose to personnel is kept as low as possible. To guide the design CMS uses an absolute annual *design limit* of 5 mSv per person.

## References

- [1] *Radiation Protection Manual*, CERN Safety Code F (1996).
- [2] P. A. Aarnio *et al*, CERN TIS-RP/168 (1986) and CERN TIS-RP/190 (1987) .  
A. Fassò *et al*, Proc IV Int. Conf. on Calorimetry in High Energy Physics, La Biodola, Sept 20-25, 1993, Ed. A. Menzione and A. Scribano, World Scientific, p. 493 (1993).  
P. Aarnio and M. Huhtinen, Proc MC93, Int. Conf. on Monte Carlo Simulation in High Energy and Nuclear Physics, p 1, ed. P. Dragowitsch, S. Linn and M. Burbank, World Scientific (1994).  
A. Fassò *at al*, Specialists' Meeting on Shielding Aspects of Accelerators, Targets and Irradiation Facilities. Arlington, Texas, April 28-29, 1994. NEA/OECD doc. p. 287 (1995).

- [3] M. Huhtinen, CERN CMS NOTE-2002/019 (2002).
- [4] P. A. Aarnio, CERN CMS NOTE-1998/086 (1998).
- [5] M. Huhtinen, CERN/TIS-RP/IR/98-28 (1998).
- [6] P. A. Aarnio, J. J. Ala-Heikkilä, T. T. Hakulinen and M. Huhtinen, *High-energy proton irradiation and induced radioactivity analysis for some construction materials for the CERN LHC*, Presented at the conference *Methods and Applications in Radioanalytical Nuclear Chemistry VI*, Kona, USA, April 7–11, 2003, to be published in *J. Radioanal. Nucl. Chem.*.
- [7] R. Thomas and G. Stevenson, *Radiological Safety Aspects of the Operation of Proton Accelerators*, IAEA Technical Reports Series 283 (1988).
- [8] K. Potter and G. R. Stevenson, CERN LHC Note 310 (1995).
- [9] The CMS Collaboration, *The Tracker Project Technical Design Report*, CERN LHCC 98-6 (1998).